Thin Solid Films 616 (2016) 698–702

Contents lists available at ScienceDirect

Thin Solid Films

journal homepage: www.elsevier.com/locate/tsf

# Fast electron transfer kinetics on novel interconnected nanospheres of graphene layers electrodes☆

A.C. Peterlevitz [a], P.W. May [b], R.L. Harniman [b], J.A. Jones [b], H.J. Ceragioli [a], H. Zanin [a,b,*]

[a] Carbon Sci-Tech Labs, Universidade Estadual de Campinas, Campinas 13 083-852, Brazil
[b] School of Chemistry, University of Bristol, Bristol BS8 1TS, United Kingdom

ARTICLE INFO

*Article history:*
Received 27 April 2016
Received in revised form 26 August 2016
Accepted 21 September 2016
Available online 22 September 2016

*Keywords:*
Sensor
Electrochemistry
Graphene
Layers
Thin film

ABSTRACT

A novel thin solid film of interconnected carbon nanospheres (ICNS) has been developed and characterized as electrode. The thin film is composed of interconnected carbon nanospheres with average crystallite size of ~5 nm and laminar graphene layers separated by an interplanar spacing of ~0.32 nm. An electrode was prepared in a one-step process by depositing ICNS onto a niobium substrate by hot filament chemical vapour deposition. To prepare an electrode, solvent-refined oil without additives was annealed up to 530 °C under ~2700 Pa of a gas mixture containing ethanol, methanol, water, and boron trioxide. The resulting ICNS film was characterized by scanning and transmission electron microscopy, plus Raman, Fourier transform infrared and energy dispersive spectroscopies. The contact angle between deionized water and the ICNS surface was zero - the water droplet instantaneously spread over the sample surface indicating a hydrophilic surface. The film behaviour as an electrochemical electrode was studied by cyclic voltammetry and electrochemical impedance spectroscopy. ICNS layers exhibited a large potential window, low uncompensated resistance, as well as low charge-transfer impedance in the presence of ferrocene-methanol or ferrocyanide as redox probes. These useful properties make ICNS electrodes very promising for future applications in electrocatalysis and (bio)sensors.



## 1. Introduction

Carbon is a very attractive material for electrochemical applications due to its different allotropes (fullerenes, nanotubes, graphene and diamond) of dimensionality from 0D to 3D [1,2]. Carbon materials can be prepared in various microtextures from powders to freestanding fibres, foams, amorphous, crystals and composites [3,4]. As an electrode material, carbon surface shows fairly low charge transfer impedance and high chemical stability in strongly acidic or basic solutions with good performance over a wide range of temperatures [5,6,7]. Carbon nanotubes [8,9], carbon nanofibres [10,11], carbon trees [12], fullerenes [13], the $C_n$ family [14], carbon onions [15,16] and carbon spheres [17] have all been investigated as an electrode material.

Among these various $sp^2$ carbon nanostructures, carbon nanospheres (CNSs) have attracted much attention because of their applications in electronic devices, catalysis, adsorbents and as anode materials in lithium-ion batteries [18–25]. To date, most of these carbon nanospheres are hollow carbon structures composed of stacked hexagonal graphene sheets linked as rings. By incorporating pentagons the flat structures eliminate all dangling bonds, enabling them to curl up to form a ball [16,17]. Fullerene, $C_n$ cage, onion-like carbon nanospheres have shells with radial graphene-like layers differing in their interplanar spacing, particle size and the numbers of both carbon atoms and shells (Fig. 1).

In this work we present a novel film of interconnected carbon nanospheres (ICNSs), which is composed of approximately a dozen laminar graphene layers. These spheres are hydrophilic and exhibit fast electron transfer in the presence of ferrocene-methanol or ferrocyanide as redox probes, which evidence their applicability as electrochemical sensors.

## 2. Experimental

### 2.1. ICNS film growth

The thin films of ICNSs were prepared on niobium disks (diameter 25 mm and thickness 2 mm) by hot filament chemical vapour deposition (HFCVD). Prior to the deposition, the substrates were polished and cleaned in an ethanol bath under sonication. After drying the samples, a drop of concentrated hydrocarbon oil (Vitrea 100 oil manufactured and sold commercially by Shell) was placed on the top surface where it spread out uniformly. The sample was then placed into a reactor chamber, which was then evacuated to a base pressure of 0.03 Pa. A gas mixture of 85 sccm of hydrogen, 15 sccm of nitrogen

☆ In memory of Prof Vitor Baranauskas.

* Corresponding author at: Carbon Sci-Tech Labs, Universidade Estadual de Campinas, Campinas 13 083-852, Brazil.
*E-mail address:* hudsonzanin@gmail.com (H. Zanin).

http://dx.doi.org/10.1016/j.tsf.2016.09.044
0040-6090/


**Fig. 1.** Schematic representation of carbon nanospheres.

and 10 sccm of the vapour from an ethanol:methanol:water (40:80:64) solution was introduced into the chamber via suitable mass flow controllers. Hydrogen gas was bubbled through this mixture carrying it into the chamber. The chamber pressure was maintained at 2600–2800 Pa throughout the deposition run. For thin film formation, a tungsten filament was position 5 mm above the sample and resistively heated up to 2000 °C measured by a pyrometer. Radiative heat from the filament heated the sample at a rate of 50 °C/min for 10 min to a temperature of ~530 °C, and this temperature was maintained for a further 30 min, after which the filament was progressively cooled down in a pure hydrogen atmosphere for 10 min. The substrate temperature was measured using a thermocouple embedded in the back side of substrate.

### 2.2. Characterization and electrochemical studies

ICNS samples were characterized by scanning electron microscopy (SEM), transmission electron microscopy (TEM), Raman spectroscopy, Fourier transform infrared (FTIR) spectroscopy, energy dispersive spectroscopy (EDS), contact angle (CA) and electrochemical tests. SEM and TEM were performed with a JEOL6330 operated at 10 kV and JEOL2011 operated at 200 kV, respectively. Raman spectra were recorded at room temperature using a Renishaw microprobe, employing UV (325 nm), green (514 nm) and near infrared (785 nm) laser excitation. Surface chemical electrodes and oil were investigated by Fourier transform infrared attenuated total reflection spectroscopy (ATR-FTIR: Spectrum Spotlight-400, Perkin-Elmer). The semi-quantitative analysis of chemical elements was performed by EDS measurements using an Inca Penta FET ×3 Oxford Instruments. A Krüss Easy-Drop system employing the sessile-drop method was used to evaluate the wettability of electrodes by measuring the CA of the ICNS layers with high-purity deionized water drops.

Cyclic voltammetry (CV) and electrochemical impedance spectroscopy (EIS) were recorded with an Autolab PGSTAT30 potentiostat. The electrochemical responses of ICNS films grown on niobium were compared with those from a niobium disk substrate using Ar-saturated aqueous electrolyte solutions containing $KNO_3$, $C_{11}H_{12}FeO$ or $K_4Fe(CN)_6$ as the supporting electrolyte and redox probe, respectively. The geometrical surface area of the working electrode was defined by using chemically inert adhesive 3 M Teflon tape to mask off some of the film, leaving a 3-mm-diameter open hole of fixed area (0.071 $cm^2$). The electrical contact was made on the top of the electrode using a crocodile clip covered by parafilm wrap. Ag/AgCl (in saturated KCl) and a pure platinum mesh were employed as reference and counter electrodes, respectively. All chemicals and supporting electrodes were purchased from Sigma Aldrich.

## 3. Results and discussion

### 3.1. Structural characterization of the ICNS layer

Fig. 2(a–c) shows electron and atomic force micrographs of the ICNS films revealing (a) interconnected quasi-spherical structures covering the whole niobium substrate; and details of (b) the topography of the sample and (c–f) the particle shape and sizes and the layered structures filling the nanospheres. Particle diameters ranged from 2.5 to 10 nm with interplanar spacing 0.32 ± 0.02 nm.

Fig. 3(a–d) shows Raman spectra from ICNS film obtained from (b) UV, 325 nm, (c) green, 514 nm and (d) near IR, 785 nm excitation wavelengths. Fig. 3(a) shows all spectra overlapped and Fig. 3(b–d) each spectrum deconvoluted. In the first-order of all Raman spectra the two main peaks are known as the D- and G-bands, assigned to $sp^2$ carbon structures. In Fig. 3 (a) the D-band centre position has shifted from 1360 to 1347 $cm^{-1}$ as excitation wavelength was changed from 785 to 514.5 nm, respectively. The D band is associated with a double resonance process involving a phonon and a defect, commonly observed in disordered nanoscale carbon phases [19]. This is consistent with the

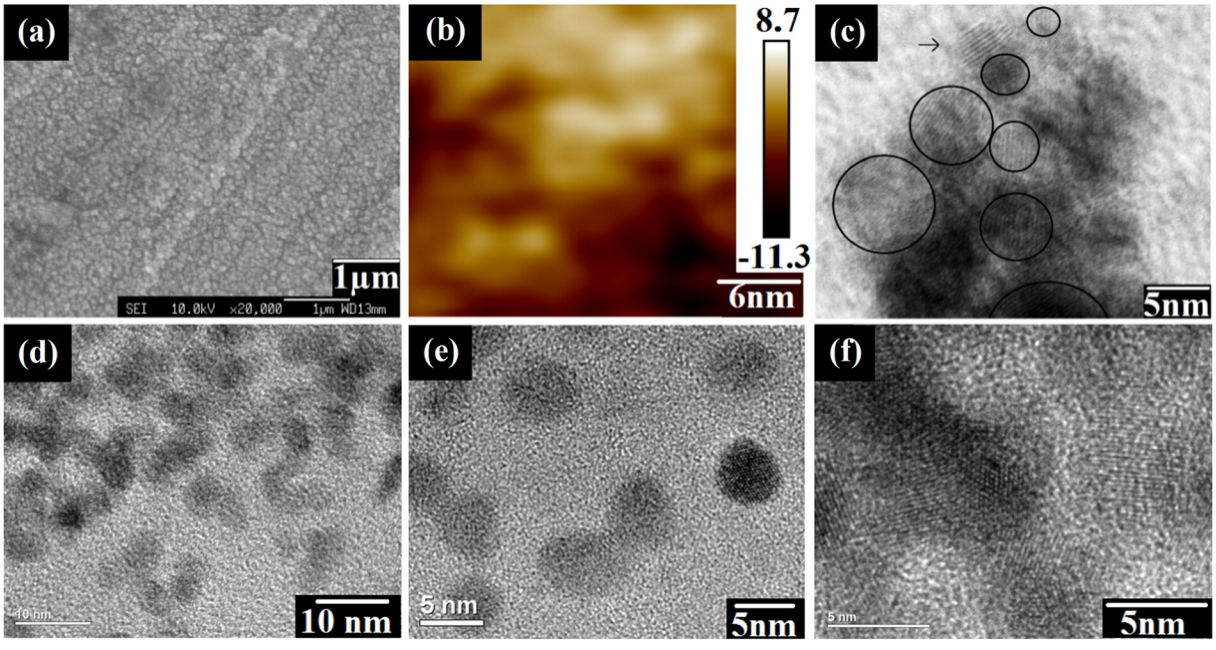


**Fig. 2.** (a) Scanning electron, (b) atomic force and (c-f) transmission electron microscope images of ICNS morphology prepared on a niobium substrate.

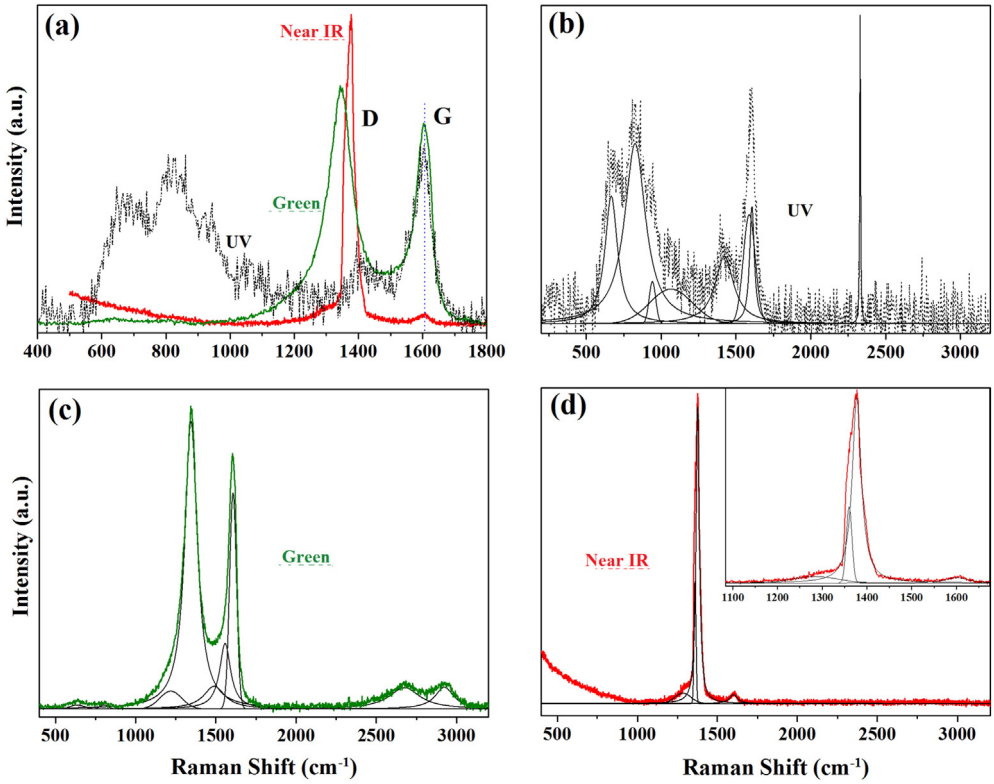


**Fig. 3.** (a) Overlapped Raman spectra of the ICNS layer measured at different excitation wavelengths (UV) 325 nm, (green) 514 nm and (near IR) 785 nm. Deconvoluted Raman spectra obtained from (b) 325 nm, (c) 514 nm and (d) 785 nm excitation wavelengths. (For interpretation of the references to color in this figure legend, the reader is referred to the web version of this article.)

SEM images showing large amounts of edges and boundaries present in the film.

The G-peak is centred at 1600 $cm^{-1}$ and does not shift with the excitation wavelength, suggesting the presence of a crystalline carbon phase. The G-band stems from in-plane vibrations and has $E_{2g}$ symmetry corresponding to stretching vibrations in the basal plane ($sp^2$ domains) of single-crystal graphene or nanocrystalline graphite.

We have observed that the ratio of the area under the D and G peaks ($A_D/A_G$) increases as the excitation laser energy ($E_L$) increases. The $A_D/A_G$ ratio is useful to calculate the average crystallite size ($L$) using Eq. (1) [20], where $E_L$ is the laser excitation energy in eV:

$$L\,(\mathrm{nm}) = \frac{560}{E_L^4}\left(\frac{A_D}{A_G}\right)^{-1} \tag{1}$$

For $E_L = 2.41$ eV (excitation by 514 nm, Fig. 3 (c)), our sample has $A_D/A_G \sim 3.5$ and thus a crystallite size ~4.8 nm, which is consistent with the TEM observations (Fig. 2(c)).

Deconvolution of the Raman spectra of ICNS films measured using 325, 514 and 785 nm excitation are shown in detail in Figs. 3(b) to (d), which exhibit features associated with the $sp^2$ and $sp^3$ carbon sites and carbon and oxygen bonds. In the first-order of all Raman spectra, besides the D- and G-bands already discussed, the feature at 1218–1273 $cm^{-1}$ has its origin in a double resonance process on graphene phonon dispersion curves [21]. From the presence of the latter mode and D- and G-band analyses, we can infer the predominance of $sp^2$ carbon in the film. The small peak at around 1060 $cm^{-1}$ (T-peak) reveals a slight content of $sp^3$ carbon [22], which only could be detected by UV excitation (Fig. 3(b)). The band centred at around 1489 $cm^{-1}$ appears on all Raman spectra and is evidence of oxygen functional groups bonded to carbon on ICNSs [23]. In summary, Raman analyses indicate mainly the presence of highly crystalline carbon, such as graphene, together with oxygen groups attached to the surface.

Fig. 4 contrasts the ATR-FTIR spectra from the ICNS film with that from the hydrocarbon oil, which was used as precursor. From the spectra we can observe the carbon-carbon and carbon-oxygen bonds. The band around 1532 $cm^{-1}$ is attributed to the C═C graphitic structure of carbon nanospheres, while the C—C bonds of the aromatic nuclei appear at both ~700 and 1200 $cm^{-1}$ [24,25]. The peaks centred at ~1250 and 1466 $cm^{-1}$ are assigned to C—O and O—H (of carboxylic groups), respectively [26,27]. The band at ~1660 $cm^{-1}$ is assigned to the C═O stretching mode in quinone groups, and the band at ~1730 $cm^{-1}$ is indicative of the C═O in carboxylic groups (COOH) [26], which is consistent with Raman analyses and EDS results (spectra not shown).

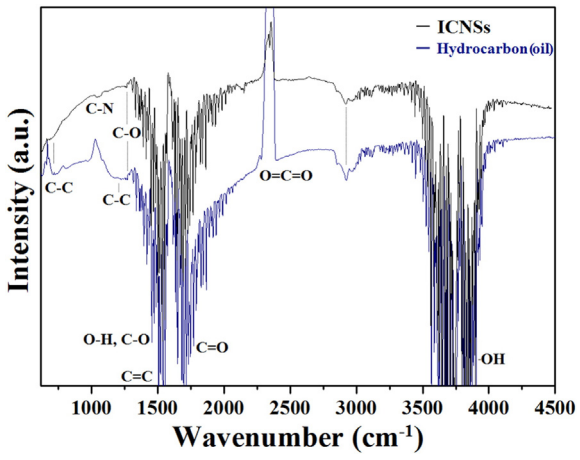


**Fig. 4.** ATR-FTIR spectra of ICNS layers and the hydrocarbon oil (Vitrea 100) used for sample preparation.

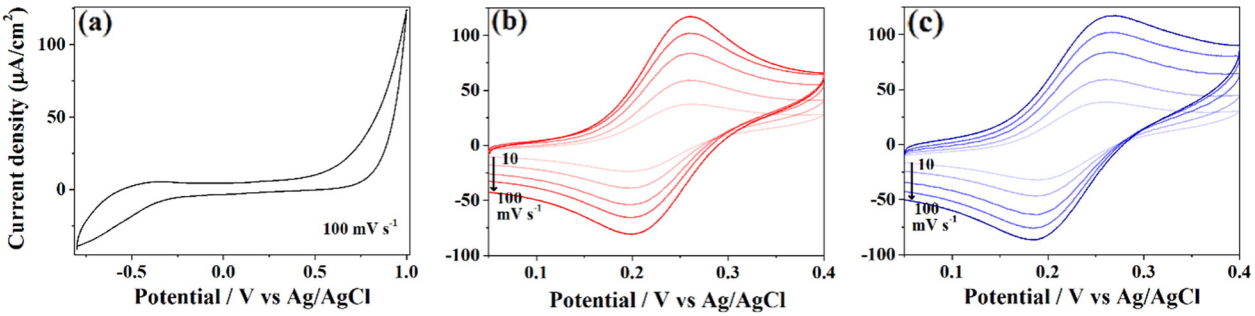


**Fig. 5.** CVs from ICNS electrodes taken in (a) 0.1 M potassium nitrate scanned at a constant 100 mV $s^{-1}$, and (b) 0.1 M potassium nitrate plus 0.5 mM ferrocene-methanol; and (c) 0.1 M potassium nitrate plus 0.5 mM ferrocyanide, taken at different scan rates (10, 25, 50 75 and 100 mV $s^{-1}$).

From EDS, we semi-quantified the atomic composition of the CNS film as ~86% carbon with the balance being oxygen. The main oxygen source is the solvent used for hydrocarbon oil refining and the alcohol (methanol and ethanol) vapours used during growth. These oxygen functional groups revealed by FTIR have polar characteristics and can interact strongly with water. The contact angle between deionized water and the ICNS surfaces is zero, where the water droplet instantaneously spreads over the sample surface, indicating an extreme hydrophilic surface. Also from FTIR spectra the band at 1030 $cm^{-1}$ represents C—N bond stretching vibrations, and is found only on ICNS samples [28], where the main source is the nitrogen gas used during growth. The band that ranges from ~2250–2390 $cm^{-1}$ is assigned to uncompensated $CO_2$ (*g*) from the air in the spectrometer. Both peaks centred at 1380 and 2920 $cm^{-1}$ are assigned as bending and stretching vibrations of C—H. The intense bands at 3400 $cm^{-1}$ indicate stretching vibrations of isolated surface —OH moieties and/or —OH in carboxyl groups in absorbed water [29]. From FTIR spectra we can conclude the oxygen functional groups are attached to the carbon in the ICNS film, changing the surface wettability of the sample. Hydrophilic carbon materials are desirable for charge transfer across an electrode/electrolyte interface.

### 3.2. Electrochemical properties of ICNS films

Cyclic voltammograms (CVs) of ICNS film electrodes are displayed in Fig. 5 showing (a) 0.1 M $KNO_3$ electrolyte solution scanned at 100 mV $s^{-1}$ and (b) 0.1 M $KNO_3$ electrolyte plus 0.5 mM ferrocene-methanol and (c) 0.1 M $KNO_3$ electrolyte plus 0.5 mM ferrocyanide as a function of the potential scan rate (10, 25, 50 75 and 100 mV $s^{-1}$). The ICNS electrode exhibits a working potential window of about 1 V, which is similar to that from standard glassy carbon or HOPG electrodes [30]. The interfacial capacitance was estimated from the current density as function of scan rate at 0.3 V in Fig. 5 (a). The double-layer capacitance was ~21 μF $cm^{-2}$ for the ICNS electrode. Compared to a typical value for a HOPG electrode of 5 μF $cm^{-2}$ [31], this correspond to a surface area increase of ~4 times.

Characteristic CVs for ICNS electrodes in the presence of the two chemical probes are shown in Fig. 5(b & c). A high degree of reversibility is observed at various scan rates. The peak current intensities are proportional to the square root of the scan rate, which means this is a diffusion-controlled process. The diffusion coefficients of the redox probes were estimated 7.4 × $10^{-6}$ $cm^2$ $s^{-1}$ for ferrocene-methanol and 7 × $10^{-6}$ $cm^2$ $s^{-1}$ for ferrocyanide based on the Randles-Sevcik equation [32].

Further evidence of the electroactive nature of the ICNS films is illustrated by the electrochemical impedance spectra shown in Fig. 6 for both chemical probes. The frequency dependence of phase is compatible with a Randles behaviour, and analysis of the impedance data based on the Randles circuit showed essentially reversible behaviour for the ICNS electrode, with an uncompensated resistance of 228 ± 9 Ω, a Warburg element $Y_o$ of 0.11 ± 0.03 × $10^{-3}$ $s^{0.5}$ $\Omega^{-1}$ (consistent with the diffusion coefficient of the redox probe) and capacitance from double-layer formation of 1.4 ± 0.5 × $10^{-6}$ F (consistent with the capacitance calculated from the CVs). The magnitude of the impedance amplitude (|*Z*|) is slightly higher for ferrocyanide compared to ferrocene-methanol, which is attributed to impedance for charge transfer ($R_{ct}$). The $R_{ct}$ value extracted from analysis of the ICNSs/ferrocyanide interface was 0.8 kΩ, whereas that from the ICNSs/ferrocene-methanol interface was negligible.

Cyclic voltammetry and impedance spectroscopy in the presence of both ferrocene-methanol and ferrocyanide as a redox probe exhibit reversible behaviour with a differential capacitance above 21 μF $cm^{-2}$.

## 4. Conclusions

We have presented a novel class of carbon nanospheres with diameters ranging from 2.5 to 10 nm and an interplanar spacing

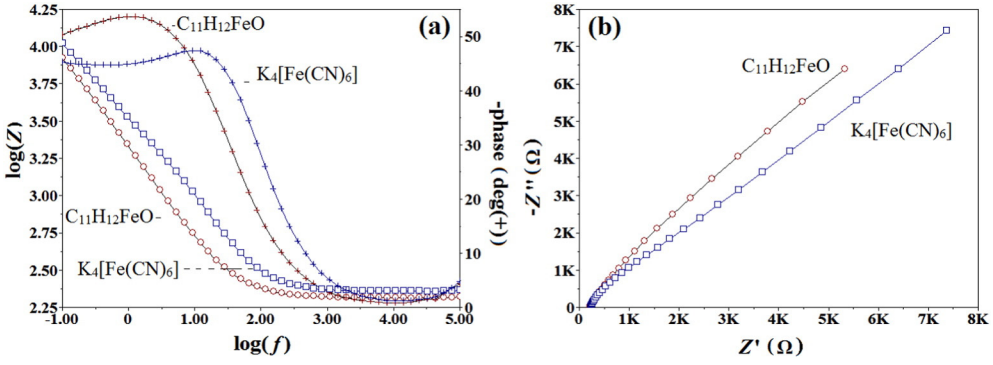


**Fig. 6.** Impedance spectra taken at 0.23 V as the frequency (*f*) is decreased from 100 kHz to 0.1 Hz for an ICNS electrode in 0.5 mM ferrocene-methanol (red ○ for impedance and + for phase) or 0.5 mM potassium ferrocyanide (blue □ for impedance and + for phase) with 0.1 M potassium nitrate aqueous solution. The data are presented as (a) Bode plots (the modulus of the impedance amplitude |*Z*| and the phase of the impedance response versus the frequency) and (b) Nyquist plots. (For interpretation of the references to color in this figure legend, the reader is referred to the web version of this article.)

0.32 ± 0.02 nm. We believe that interplanar spacing is slightly lower than graphite due to internal stress of spherical configuration. However, this is a complex topic. For instance, literature showed that the spacing values of DWCNTs and MWCNTs vary from 0.27 up to 0.42 nm [33]. The most common values are in the range of 0.32–0.35 nm and do not strongly depend on the synthesis method. In particular, it was indicated that the stability of a CNT depends only on the interlayer spacing, which reaches an energy minimum when the mean interlayer separation is 0.34. In our case, the interplanar spacings are very similar ranging from 0.30 to 0.34 nm, suggesting that electrostatic interactions between partially charged atomic centres, which exist in our sample and are probably absent in graphite. These interconnected conducting spheres have a low production cost and show fast charge-transfer rate in the presence of ferrocene-methanol or ferrocyanide as a redox probes. The thin films are fairly well adherent to the substrate. The capacitance is about 21 μF/cm$^2$ which is similar to that of HOPG (5 μF/cm$^2$). The difference observed is probably due to the substrate roughness. These useful properties make ICNS electrodes very promising for future electrochemical applications as sensitive electrodes.

## Acknowledgements

We gratefully acknowledge the University of Bristol School of Chemistry electron microscopy unit for TEM and the British Council, Brazilian agencies Fapesp (2014/02163-7) and the Royal Society for Newton Travel fund NI140181 for financial support. PeakForce atomic force microscopy was carried out in the Chemical Imaging Facility, University of Bristol with equipment funded by EPSRC under “Atoms to Applications” Grant ref. (EP/K035746/1).

## References

[1] E. frackowiak, F. Beguin, Carbon materials for the electrochemical storage of energy in capacitors, Carbon 39 (6) (2001) 937–950.
[2] H. Zanin, P.W. May, A.O. Lobo, E. Saito, J.P.B. Machado, G. Martins, et al., Effect of multi-walled carbon nanotubes incorporation on the structure, optical and electrochemical properties of diamond-like carbon thin films, J. Electrochem. Soc. 161 (5) (2014) H290–H295.
[3] M. Terrones, Science and technology of the twenty-first century: synthesis, properties and applications of carbon nanotubes, Annu. Rev. Mater. Res. 33 (2003) 419–501.
[4] H. Zanin, A. Margraf-Ferreira, N.S. da Silva, F.R. Marciano, E.J. Corat, A.O. Lobo, Graphene and carbon nanotube composite enabling a new prospective treatment for trichomoniasis disease, Mater. Sci. Eng., C-Mater. Biol. Appl. 41 (2014) 65–69.
[5] R.S. Borges, A.L.M. Reddy, M.-T.F. Rodrigues, H. Gullapalli, K. Balakrishnan, G.G. Silva, et al., Supercapacitor operating at 200 degrees Celsius, Sci. Rep. 3 (2013).
[6] P.H. Chen, R.L. McCreery, Control of electron transfer kinetics at glassy carbon electrodes by specific surface modification, Anal. Chem. 68 (22) (1996) 3958–3965.
[7] J.M. Nugent, K.S.V. Santhanam, A. Rubio, P.M. Ajayan, Fast electron transfer kinetics on multiwalled carbon nanotube microbundle electrodes, Nano Lett. 1 (2) (2001) 87–91.
[8] M.A.V.M. Grinet, H. Zanin, A.E. Campos Granata, M. Porcionatto, F.R. Marciano, A.O. Lobo, Fast preparation of free-standing nanohydroxyapatite-vertically aligned carbon nanotube scaffolds, J. Mater. Chem. B 2 (9) (2014) 1196–1204.
[9] T.W. Ebbesen, P.M. Ajayan, Large-scale synthesis of carbon nanotubes, Nature 358 (6383) (1992) 220–222.
[10] K.P. De Jong, J.W. Geus, Carbon nanofibers: Catalytic synthesis and applications, Catal. Rev. Sci. Eng. 42 (4) (2000) 481–510.
[11] R.L. Vander Wal, T.M. Ticich, V.E. Curtis, Directed synthesis of metal-catalyzed carbon nanofibers and graphite encapsulated metal nanoparticles, J. Phys. Chem. B 104 (49) (2000) 11606–11611.
[12] P.M. Ajayan, J.M. Nugent, R.W. Siegel, B. Wei, P. Kohler-Redlich, Growth of carbon micro-trees - carbon deposition under extreme conditions causes tree-like structures to spring up, Nature 404 (6775) (2000) 243-.
[13] D.L. Lichtenberger, K.W. Nebesny, C.D. Ray, D.R. Huffman, L.D. Lamb, Valence and core photoelectron-spectroscopy of $C_{60}$, buckminsterfullerene, Chem. Phys. Lett. 176 (2) (1991) 203–208.
[14] Q.L. Zhang, S.C. Obrien, J.R. Heath, Y. Liu, R.F. Curl, H.W. Kroto, et al., Reactivity of large carbon clusters - spheroidal carbon shells and their possible relevance to the formation and morphology of soot, J. Phys. Chem. 90 (4) (1986) 525–528.
[15] V.L. Kuznetsov, A.L. Chuvilin, Y.V. Butenko, I.Y. Malkov, V.M. Titov, Onion-like carbon from ultra-disperse diamond, Chem. Phys. Lett. 222 (4) (1994) 343–348.
[16] J.Y. Miao, D.W. Hwang, K.V. Narasimhulu, P.-I. Lin, Y.-T. Chen, S.-H. Lin, L.-P. Hwang, Synthesis and properties of carbon nanospheres grown by CVD using Kaolin supported transition metal catalysts, Carbon 4 (2004) 813–822.
[17] D. Ugarte, Curling and closure of graphitic networks under electron-beam irradiation, Nature 359 (1992) 707–709.
[18] X. Zhang, Y. Cui, Z. Lv, M. Li, S. Ma, Z. Cui, Q. Kong, Carbon nanotubes, conductive carbon black and graphite powder based paste electrodes, Int. J. Electrochem. Sci. 6 (2011) 6063–6073.
[19] V. Carozo, C.M. Almeida, E.H.M. Ferreira, L.G. Cancado, C.A. Achete, A. Jorio, Raman signature of graphene superlattices, Nano Lett. 11 (11) (2011) 4527–4534.
[20] L.G. Cancado, K. Takai, T. Enoki, M. Endo, Y.A. Kim, H. Mizusaki, et al., General equation for the determination of the crystallite size $L_a$ of nanographite by Raman spectroscopy, Appl. Phys. Lett. 88 (16) (2006).
[21] M.S. Dresselhaus, A. Jorio, M. Hofmann, G. Dresselhaus, R. Saito, Perspectives on carbon nanotubes and graphene Raman spectroscopy, Nano Lett. 10 (3) (2010) 751–758.
[22] A.C. Ferrari, Determination of bonding in diamond-like carbon by Raman spectroscopy, Diam. Relat. Mater. 11 (3–6) (2002) 1053–1061.
[23] A.O. Lobo, A. SC, A. EF, M. FR, T.-A. VJ, C. EJ, Fast functionalization of vertically aligned multiwalled carbon nanotubes using oxygen plasma, Mater. Lett. 70 (2012) 89–93.
[24] M.H. Liu, Y.L. Yang, T. Zhu, Z.F. Liu, Chemical modification of single-walled carbon nanotubes with peroxytrifluoroacetic acid, Carbon 43 (7) (2005) 1470–1478.
[25] J.E. Huang, X.H. Li, J.C. Xu, H.L. Li, Well-dispersed single-walled carbon nanotube/polyaniline composite films, Carbon 41 (14) (2003) 2731–2736.
[26] D.C. Marcano, D.V. Kosynkin, J.M. Berlin, A. Sinitskii, Z. Sun, A. Slesarev, et al., Improved synthesis of graphene oxide, ACS Nano 4 (8) (2010) 4806–4814.
[27] Y. Estevez-Martinez, C. Velasco-Santos, A.-L. Martinez-Hernandez, G. Delgado, E. Cuevas-Yanez, D. Alaniz-Lumbreras, et al., Grafting of Multiwalled Carbon Nanotubes with Chicken Feather Keratin, Journal of Nanomaterials (2013) (Missing volume no, and pages).
[28] T. Ramanathan, F.T. Fisher, R.S. Ruoff, L.C. Brinson, Amino-functionalized carbon nanotubes for binding to polymers and biological systems, Chem. Mater. 17 (6) (2005) 1290–1295.
[29] L. Stobinski, B. Lesiak, L. Koever, J. Toth, S. Biniak, G. Trykowski, et al., Multiwall carbon nanotubes purification and oxidation by nitric acid studied by the FTIR and electron spectroscopy methods, J. Alloys Compd. 501 (1) (2010) 77–84.
[30] G.M. Swain, The susceptibility to surface corrosion in acidic fluoride media - a comparison of diamond, hopg, and glossy carbon electrodes, J. Electrochem. Soc. 141 (12) (1994) 3382–3393.
[31] C.R. Bradbury, L. Kuster, D.J. Fermin, Electrochemical reactivity of HOPG electrodes modified by ultrathin films and two-dimensional arrays of metal nanoparticles, J. Electroanal. Chem. 646 (1–2) (2010) 114–123.
[32] T.A. Silva, H. Zanin, E. Saito, R.A. Medeiros, F.C. Vicentini, E.J. Corat, O. Fatibello-Filho, Electrochemical behaviour of vertically aligned carbon nanotubes and graphene oxide nanocomposite as electrode material, Electrochim. Acta 119 (2014) 114–119.
[33] O.V. Kharissova, B.I. Kharisov, Variations of interlayer spacing in carbon nanotubes, RSC Adv. 4 (2014) 30807–30815.